Soft Matter

Cite this: *Soft Matter*, 2012, **8**, 11613

www.rsc.org/softmatter

PAPER

Shapes of pored membranes

Zhenwei Yao, Rastko Sknepnek, Creighton K. Thomas and Monica Olvera de la Cruz*

Received 10th July 2012, Accepted 18th September 2012
DOI: 10.1039/c2sm26608c

We study the shapes of pored membranes within the framework of the Helfrich theory under the constraints of fixed area and pore size. We show that the mean curvature term leads to a budding-like structure, while the Gaussian curvature term tends to flatten the membrane near the pore; this is corroborated by simulation. We propose a scheme to deduce the ratio of the Gaussian rigidity to the bending rigidity simply by observing the shape of the pored membrane. This ratio is usually difficult to measure experimentally. In addition, we briefly discuss the stability of a pore by relaxing the constraint of a fixed pore size and adding the line tension. Finally, the flattening effect due to the Gaussian curvature as found in studying pored membranes is extended to two-component membranes. We find that sufficiently high contrast between the components' Gaussian rigidities leads to budding which is distinct from that due to the line tension.

1. Introduction

The cell membrane is a complex bilayer sheet consisting of hundreds of lipid species embedded with numerous surface- and trans-membrane proteins.[1] Its main role is to separate the cell's interior from its surroundings and to act as a conduit for exchanging matter and signaling between the cell and its environment. The cell membrane is a dynamic object whose conformational variations are associated with biological activities such as cell fission, fusion, and adsorption.[2] Most biological membranes exist in a liquid state where lipid molecules are rather strongly confined to the bilayer plane but can easily diffuse laterally within it. Fluidity allows the membrane to dynamically rearrange its local composition, quickly heals holes, and enables transmembrane transport besides allowing other metabolic functions. A substantial portion of the transport through the cell membrane takes place *via* pores.[3,4] The presence of a pore changes the topology of a membrane and can significantly influence its conformations and functions.[5] Characterizing the conformations of closed membranes has been a subject of active research over the past four decades with numerous experimental[6,7] and theoretical[8–10] studies.

Despite a high molecular complexity, when the length scale is large compared to the bilayer thickness and the energy scale is small compared to the typical intermolecular interactions, the cell membrane shape can be successfully described by a simple model proposed by Helfrich nearly forty years ago.[11] In his seminal paper, Helfrich argued that the low-energy large-scale properties of a liquid membrane can be described in terms of a free energy that is a quadratic function of the two principal curvatures expressed in terms of their two invariants: the mean curvature and the Gaussian curvature. Within the framework of the Helfrich theory, various axisymmetric and non-axisymmetric shapes of closed membranes have been predicted.[12,13] In particular, the longstanding physiological puzzle about the biconcave shape typical of the red blood cells has been beautifully solved; the shape of the red blood cells has been understood as the conformation that minimizes the Helfrich free energy under a set of prescribed volume and area constraints.[14] Many predictions based on the Helfrich free energy have been observed experimentally.[9] For example, the theoretical discovery of the thermal repulsion between membranes, that is to prevent sticking of cells, has been confirmed by small angle X-ray diffraction experiments.[11,15]

There are various ways to form pores on membranes *in vivo* and *in vitro*. For example, pore-forming toxin proteins exist in a wide range of organisms including bacteria, fungi, plant and animal cells.[16] By binding at particular sites on a membrane, toxins can create pores *via* oligomerizing on the membrane surface. The pores created by toxin proteins are of limited sizes. For example, the maximum size of the pore formed by SecYEG on *E. coli* is below 2.2–2.4 nm.[17] Recent studies have shown that larger pores can be created on a fluid membrane by detergents[18] or submembranous protein talin.[5] Note that the size of the pore is controlled by tuning the talin concentration over an appropriate range.[18] The localization of talin mainly along the pore rim, as observed by fluorescent labelling, is likely responsible for stabilizing the pores. A recent experiment introduced a method to create pores of about 15 nm on a lipid membrane.[19] In a salt-free catanionic solution, charged pores are produced on membranes due to the partial segregation of the anionic surfactant in excess. In this case, the size of a pore can be controlled by tuning the relative amount of anionic and cationic surfactants and thus the

Department of Materials Science and Engineering, Northwestern University, Evanston, Illinois, 60208-3108, USA. E-mail: m-olvera@northwestern.edu

charges on a pore. The size of a stable pore is determined by the competition of the line tension energy γR and the electrostatic self-energy $q^2/(\varepsilon R)$, where γ is the line tension, R is the size of the pore, q is the total charge on the pore and ε is the dielectric constant of the medium, such that $R \sim \sqrt{q^2/(\gamma\varepsilon)}$. Both the increase of charge and the decrease of line tension can enlarge a pore on the membrane.

In this paper, we study how a pore modifies the morphology of a fluid membrane within the framework of the Helfrich theory. We discuss the equilibrium solutions of the Helfrich shape equation for fluid membranes with fixed area and pore size. In experiments the fixed pore size constraint can be realized by introducing stabilizing agents as discussed above. We find a budding structure in pored membranes, dictated by the mean curvature term in the Helfrich free energy. In studies of the conformation of closed single-component liquid membranes, the Gaussian curvature term in the Helfrich free energy can be omitted, as it is a constant that does not depend on the membrane's shape. However, this is no longer the case if pores are present. We show that the Gaussian curvature term can significantly influence the shape of a pored membrane by imposing a local constraint on the shape of the membrane near the pore. The Gaussian curvature term tends to pull the membrane outside a pore to the plane where the pore loop lies and the membrane near the pore is flattened. This observation may lead to a simple method to fabricate polyhedral buckled membranes by manipulating the size and position of the pores. In addition, we propose a scheme to find the ratio of the Gaussian rigidity and the bending rigidity from the shape of a pored membrane. This ratio is usually difficult to measure experimentally.[20] The proposed scheme successfully passes the test on a pored membrane generated by Surface Evolver,[21,22] and is applied in an experimental case. Furthermore, we briefly discuss the stability of a pore on a membrane by relaxing the constraint of fixed pore size and adding the line tension. We find that a budding pore may be meta-stable with a very shallow energy barrier and over a very narrow range of values of line tension. Therefore, stabilizing agents like talin proteins used in the experiment of ref. 5 are essential for a stable pore on fluid membranes. Finally, the flattening effect due to the Gaussian curvature as found in studying pored membranes is extended to two-component membranes. Multicomponent membranes can have a wide variety of morphologies, as has been recently discussed for both liquid[23,24] and polymerized membranes.[25–27] We find that the flattening effect due to the Gaussian curvature can induce budding in two-component membranes when there is sufficiently high contrast between the components' Gaussian rigidities. This is recognized as a domain-induced budding, but *via* a mechanism that is distinct from the conventional line tension driven budding.[28,29]

2. Model

The bending energy of a fluid membrane is modeled by the Helfrich free energy:[11]

$$E = \frac{1}{2}\kappa\int(2H)^2 \mathrm{d}A + \kappa_G \int K_G \mathrm{d}A, \qquad (1)$$

where κ ($\sim 10 k_B T$)[30] and κ_G are the bending rigidity and the Gaussian rigidity, respectively. The mean curvature $2H = 1/R_1 + 1/R_2$ and the Gaussian curvature $K_G = 1/(R_1 R_2)$, where R_1 and R_2 are the radii of principal curvatures. For real membranes, $\kappa > 0$ and $\kappa_G < 0$.[31] Note that in eqn (1) we have assumed that the spontaneous curvature $H_0 = 0$, as is the case if there is no asymmetry with respect to the middle surface of the bilayer. The negative sign of the Gaussian rigidity indicates that it favors lower genus surfaces.[32] For example, without considering the mean curvature term, a spherical membrane is more stable than a toroidal membrane; the integrals of the Gaussian curvature for sphere and torus are 4π and zero, respectively.

According to the Gauss–Bonnet theorem, the integral of the Gaussian curvature over a manifold M is related to the integral of the geodesic curvature k_g along the boundary of the manifold ∂M by

$$\int_M \mathrm{d}A K_G = 2\pi\chi(M) - \oint_{\partial M} k_g \mathrm{d}l \qquad (2)$$

where $\chi(M)$ is the Euler characteristic of the manifold M.[32] For a closed manifold M without pores, the geodesic curvature term vanishes and the integral of the Gaussian curvature becomes a constant. Therefore, κ_G plays no role for a topologically spherical membrane. However, κ_G becomes important if a pore is introduced into a membrane to change its topology.[32] In fact, we find that even without considering the Gaussian curvature term in the Helfrich free energy, a pore on a membrane can induce an interesting budding structure.

3. Results and discussion

3.1. Single pore

By exclusively considering the mean curvature term in the Helfrich free energy (eqn (1)), we analyze how the morphology of a topologically spherical membrane is influenced by a pore. Based on the intuition about closed membranes, one might guess that a punctured membrane would take a spherical shape everywhere except at the pore for minimizing the mean curvature term in the Helfrich free energy, as in Fig. 1(a). Numerical experiments performed with Surface Evolver,[21,22] however, show that a budding pore appears, as in Fig. 2(a). It is thus natural to ask: why does budding of the pore appear? How does such a conformation minimize the integral of the squared mean curvature? To address these questions, we compare the energies of the two shapes shown in Fig. 1(a) and (b). In order to minimize the integral of the squared mean curvature, the neck prefers to being a minimal surface with a vanishing mean curvature. A catenoid is the only minimal surface with rotational symmetry.[33]

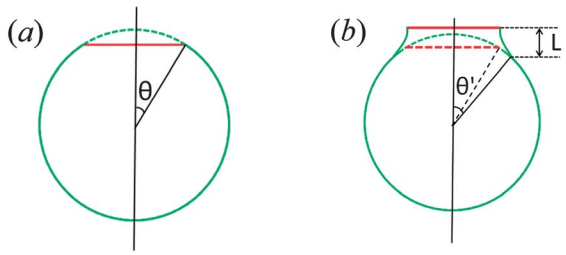

Fig. 1 The mean curvature term in eqn (1) gives rise to a budding pore (right) instead of making a membrane spherical everywhere (left). The red line represents the opening of the membrane.

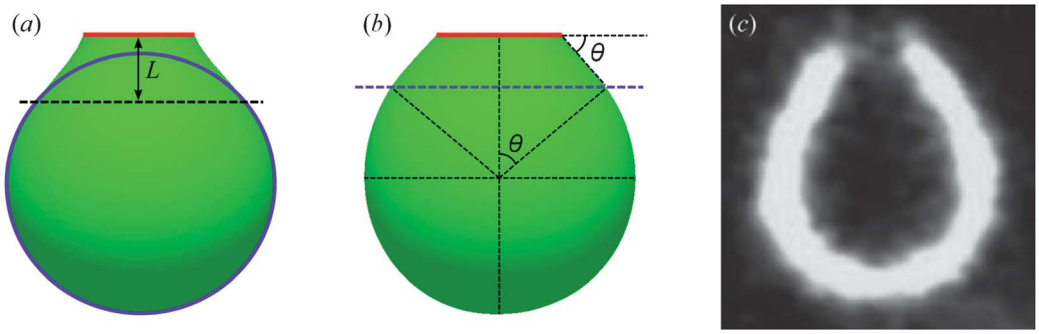

Fig. 2 The ground state shapes of a pored membrane generated by Surface Evolver. The red line represents the opening of the membrane. The size of the pore is fixed. In (a) $\kappa_G/\kappa = 0$ and in (b) $\kappa = 2$ and $\kappa_G = -1.5$. The comparison of (a) and (b) shows that the mean curvature term in the Helfrich free energy leads to a budding pore, while the Gaussian curvature term tends to flatten the membrane near the pore. In (a), measured by the radius of the pore, the radius of the sphere $R \approx 4.95$, and the longitudinal size of the budding pore $L \approx 1.22$, which agrees well with our prediction (see eqn (4)). (c) The shape of a pored fluid membrane from the experiment whose radius is about 1 μm. The pore is created by protein talin.[5] Copyright (1998) National Academy of Science, USA.

Consequently, the shape shown in Fig. 2(a) is, to first approximation, composed of a catenoid and part of a sphere (emphasized by the purple oval in Fig. 2(a)). The integrals of the squared mean curvature of the two shapes in Fig. 1 are calculated as: $E_a = \frac{\pi}{2}(1+\cos\theta)$ and $E_b = \frac{\pi}{2}(1+\cos\theta')$, where the angles θ and θ' are defined in Fig. 1. Note that the bending energy is independent of the radius of the sphere, as the integral of the squared mean curvature is a scale invariant.[8] Since $\theta' > \theta$ and $E_b < E_a$, a budding pore is preferred. A theoretical model based on the boundary layer method shows that catenoidal necks between two asymptotically flat parallel membranes (a wormhole like structure, see Fig. 3) interact like a gas of free particles with a hard-core repulsion.[7] The repulsion between necks comes from their overlap as they approach each other, which increases the bending energy of the system. It is analogous to the capillary interaction between particles floating or immersing on a liquid interface; their interaction originates from the overlap of the capillary deformations near particles.[34] Considering that the budding pore structure is half of the wormhole like structure, we expect that these budding pores also repel each other on the membrane as they approach.

We further calculate the longitudinal size L of a budding pore, as defined in Fig. 1(b). We choose an x–y coordinate system such that the x-axis is along the solid red line in Fig. 1(b) and the y-axis is along the symmetric axis of the membrane. The shape of the neck is characterized by $x(y) = r\cosh y$, where r is the radius of the waist of the catenoid. By assuming that the boundary of the pore falls on the waist of the catenoid, we obtain the expression for the angle α between the x-axis and the tangent vector at the connecting circle of catenoid and sphere: $\cot\alpha = \sinh(L/r)$. On the other hand, a geometric argument leads to the relationship between the radius R of the sphere and the size of the pore L as $R\sin\alpha = r\cosh(L/r)$. From these two expressions, we finally have

$$R = r\cosh^2\left(\frac{L}{r}\right), \tag{3}$$

where r is the radius of the pore. The dependence of the radius R of sphere on the longitudinal size L of the budding pore is plotted in Fig. 4. Measured in units of the radius of the pore, L increases from 1.4 to 1.8 as R increases from 5 to 10. Budding of a pore is more obvious in a bigger membrane. For the shape generated by Surface Evolver as shown in Fig. 2(a), we measure $R = 4.95$ and $L \approx 1.22$ which is close to our prediction $L = 1.4$. The deviation comes from the assumption that the pore boundary falls on the waist of the catenoid, which is not precisely the case in Fig. 2(a). For very large values of R, from eqn (3), the longitudinal size L of the budding pore scales as $L \sim \frac{1}{2}\ln R$. The logarithm function comes from the exponential growth of the catenoidal neck from its waist.

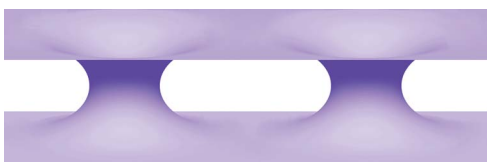

Fig. 3 The necks between two asymptotically flat parallel membranes repel each other as they approach; their overlap increases the bending energy of the system.

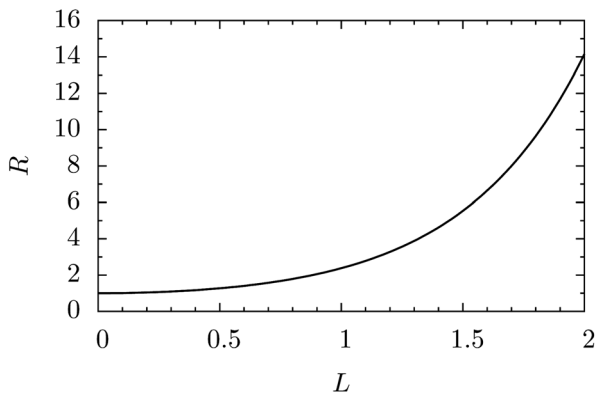

Fig. 4 Sphere radius, R, as a function of the longitudinal size L of the budding pore when $|\kappa_G| \ll \kappa$, as given in eqn (3).

In real fluid membranes, the Gaussian rigidity can contribute more than 400 kJ mol^{-1} in topological transformation of a membrane like creating a pore.[20] Theoretical microscopic models of monolayer fluid membranes show that $\kappa_G/\kappa \in [-1,0]$.[35] Therefore, the Gaussian rigidity can compete with the bending rigidity for influencing the shape of a pored membrane. In the following, we study this problem in the light of the Gauss–Bonnet theorem.

The Gauss–Bonnet theorem (eqn (2)) implies that the integral of the Gaussian curvature can be maximized by minimizing the line integral of the geodesic curvature, such that the bending energy is minimized as κ_G is negative. Therefore, the Gaussian curvature term in the Helfrich free energy, which is an integral over the whole surface, essentially imposes a local constraint on the shape near the boundary, such that the integral of the geodesic curvature on the boundary is minimized. The geodesic curvature k_g describes the deviation of a curve away from a geodesic, a generalization of a straight line in a plane. For example, the geodesic curvature of a big circle on a sphere is zero, since it corresponds to a straight line on the spherical geometry. The geodesic curvature of a curve in a surface is defined in the following way. Consider a curve $\vec{x}(s)$ being parametrized by the arc length s, its curvature is $\vec{k} = \frac{\mathrm{d}\hat{t}}{\mathrm{d}s}$, where $\hat{t} = \frac{\mathrm{d}\vec{x}}{\mathrm{d}s}$ is the unit tangent vector of the curve. For a curve on a surface equipped with the coordinates $\{\vec{e}_u,\vec{e}_v\}$, the curvature $\vec{k}$ can be projected along the normal and the tangent plane of the surface:

$$\vec{k} = \frac{\mathrm{d}\vec{t}}{\mathrm{d}s} = \vec{k}_n + \vec{k}_g, \tag{4}$$

where $\vec{k}_n = (\vec{k})_{\hat{n}}$ and $\vec{k}_g = (\vec{k})_{\mathrm{TM}}$. $\vec{n}$ is the normal vector pointing *outward*; *i.e.*, along the direction of $\vec{e}_u \times \vec{e}_v$. TM represents the tangent plane. In the Gauss–Bonnet theorem, the sign of the geodesic curvature needs to be clarified. $k_g = \vec{k}_g \cdot \hat{u}$, where $\hat{u} = \hat{n} \times \hat{t}$.[32] The direction of $\hat{t}$ is chosen to be along the boundary of the pore such that the membrane stays on the left hand side of the boundary.[32] Under these conventions, the sign of the geodesic curvature is unambiguously determined.

Using arguments based on the Gauss–Bonnet theorem, we show that the Gaussian curvature term in the Helfrich free energy tends to flatten the membrane near the pore. We first calculate the geodesic curvatures on the circular boundaries in the cut unit sphere as in Fig. 5(a). For the upper bigger part of the cut sphere, the tangent vector on the boundary circle is clockwise seen from below, so the sphere is on the left hand side walking along the boundary circle. The other tangent vector $\hat{u}$ points upward, as shown in Fig. 5(a), because the normal vector points outward. The curvature vector $\vec{k}$ of the boundary circle and the vector $\hat{u}$ make an obtuse angle, so that the geodesic curvature at any point on the boundary circle is negative $k_g = \vec{k} \cdot \hat{u} = -\frac{\sqrt{1-r^2}}{r}$, where r is the radius of the boundary circle. A similar argument shows that the sign of the geodesic curvature at the boundary of the lower smaller part of the cut sphere in Fig. 5(a) is positive. Fig. 5(b) lists all the possible shapes around a symmetric circular pore of radius r and the geodesic curvature for each case. The first shape has the minimum geodesic curvature, so it is preferred to other shapes. Therefore, the Gaussian curvature term in the Helfrich free energy tends to pull the membrane outside a pore to the plane where the pore loop lies. This conclusion also holds for multi-pored membranes. From the aspect of the Gauss–Bonnet theorem, the flattening effect of the Gaussian curvature term is disclosed. It also sheds light on the numerically generated flat surface in the vicinity of a pore on a membrane when the Gaussian rigidity is tuned to be negative.[36]

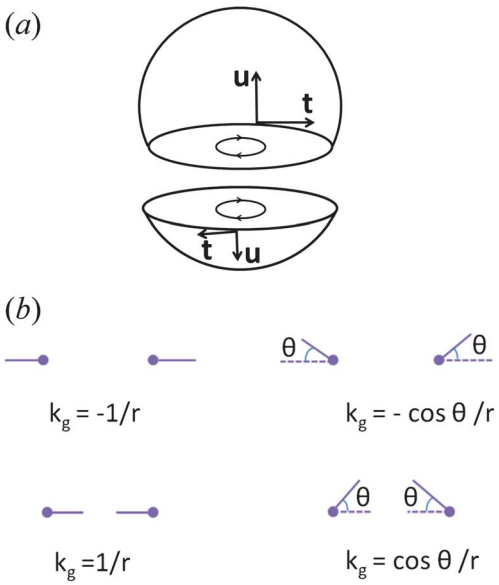

Fig. 5 (a) The calculation of the geodesic curvature. (b) Possible shapes of a membrane near a circular pore which is represented by two dots.

We use Surface Evolver to generate the ground state shape of a pored membrane for exploring the flattening effect caused by the Gaussian curvature term in the Helfrich free energy. Surface Evolver evolves a surface toward a local minimum energy shape by calculating the force on each vertex from the gradient of the total energy, which gives the direction of motion in the membrane's configuration space.[22] Therefore, the method to generate a ground state shape by Surface Evolver is distinct from that used in ref. 36, where the equilibrium shapes are produced from solving the shape equation. The result is shown in Fig. 2(b) for $\kappa = 2$ and $\kappa_G = -1.5$. A comparison of Fig. 2(a) and (b) shows that the Gaussian rigidity does play a role in regulating the shape of a pored membrane. The mean curvature term prefers to form a neck while the Gaussian curvature term tends to flatten the membrane near the pore. A dark-field micrograph of an experiment on a liposome with a pore whose size (measured by the radius of the spherical body) is similar to that in Fig. 2(b) is shown in Fig. 2(c).[5] The similarity of the shapes in Fig. 2(b) and (c) suggests that the experimental shape also results from the competition of the mean curvature and the Gaussian curvature terms.

The shape of the pore, as the result of the competition of the mean curvature and the Gaussian curvature terms, encodes the information about the ratio κ_G/κ, as has been discussed in ref. 31, 37 and 38. Note that the absolute values of these rigidities cannot be derived from the shape, because the shape is determined only by their ratio. Here, we propose a scheme to determine the quantitative relationship between the shape of the pore and the ratio κ_G/κ. Since the Gaussian curvature term flattens the

membrane near a pore, we approximate the shape in Fig. 2(b) as a combination of a circular truncated cone (the section between the red line and the purple line) and a spherical crown. The whole shape is characterized by three parameters r, A, and θ, where r is the radius of the pore, A is the area of the membrane, and θ is defined in Fig. 2(b), which is referred to as *the pore angle*. The pore angle reflects the flatness of the membrane near the pore. The total bending energy is $E_b(r, A, \theta; \kappa_G/\kappa) = \frac{1}{2}\kappa \int 2H^2 dA + k_G 2\pi(1+\cos\theta)$. The mean curvature for sphere is $2H = 2/R$ and for cone $2H = \frac{\cos^2\delta}{z\sin\delta}$, where 2δ is the cone angle and z is the vertical distance to the tip of the cone. In $E_b(\theta,r,A;\kappa_G/\kappa)$, by specifying r, A (as measured from a given shape) and κ_G/κ, we can find an optimal pore angle θ that minimizes the energy. We tune the ratio κ_G/κ for fitting the optimal pore angle to the measured one. The ratio κ_G/κ is thus found from a given shape. This scheme has its significance in application, considering that the ratio κ_G/κ is usually very difficult to measure from experiments where only a few results are available.[20] On the other hand, the scheme may be generalized to other systems, where the direct measurement of the elastic moduli is difficult, like for living materials.[39,40]

We test the above method for finding the ratio κ_G/κ of the shape shown in Fig. 2(b). The radius of the pore is defined as unity, so $R = 2.3$ and the area is calculated to be 62.8. By varying the ratio κ_G/κ, we get different optimal pore angles, as shown in Fig. 6(a). It shows that the membrane near the pore becomes more and more flatten (θ decreases) with stronger flattening effect by the Gaussian curvature term (the absolute value of κ_G/κ increases). For fitting the optimal angle to the measured pore angle 47°, the ratio is required to be $\kappa_G/\kappa = -0.75$, which is exactly the one we use in Surface Evolver to generate the shape in Fig. 2(b). The validity of the scheme for obtaining the ratio κ_G/κ is thus substantiated.

Now we apply this scheme to the shape in Fig. 2(c) for identifying the ratio κ_G/κ of the liposome used in the experiment of ref. 5. From the experimental shape shown in Fig. 2(c), we measure $R = 2.25$, pore angle $\theta = 55°$ and calculate the area $A = 66$. It is found that the observed pore angle can be fitted by using $\kappa_G/\kappa = -0.45$. Therefore, the value of the ratio κ_G/κ of the liposome in the experiment of ref. 5 was estimated to be -0.45, which was of the same order as the experimentally known values for typical liposomes.[20]

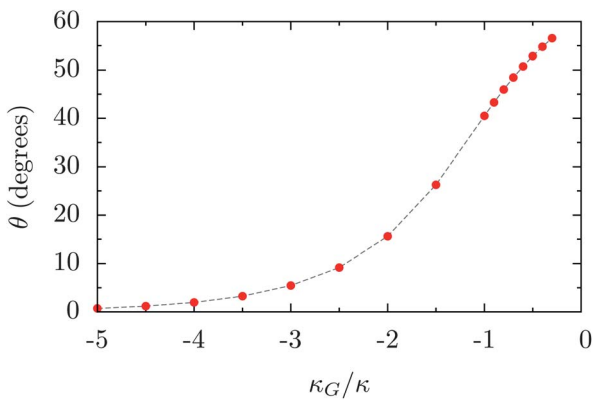

Fig. 6 The plot of optimal pore angle θ *vs.* the ratio of κ_G/κ. The area was measured to be 62.8 from the shape shown in Fig. 2(b) where the fixed radius of the pore is defined to be unity. The membrane near the pore becomes more and more flatten (θ decreases) with the increase of the absolute value of κ_G/κ. For a real fluid membrane, $\kappa_G/\kappa \in [-1,0]$, where more points are plotted.

3.2. Stability of a pore with line tension

Finally, we briefly discuss the consequences of relaxing the constraint of fixed pore size by introducing the line energy, $\gamma \oint_\partial dl$ for the pore.[47] We explore the stability of a budding pore by working in the regime of $|\kappa_G| \ll \kappa$ where the formation of a budding structure is expected. The pored membrane is assumed to take the shape of a spherical cap plus a catenoid, and the boundary of the pore is approximated as falling on the waist of the catenoid. The energy is thus obtained as $E = \frac{\pi\kappa}{4}(1+\cos\theta) + \gamma 2\pi r + \kappa_G 2\pi$, where θ is the pore angle and r is the radius of the pore. The area of the pore membrane is fixed: $A = \pi r(2L + r\sinh(2L/r)) + 2\pi R^2(1+\cos\theta)$, where L is the height of the pore and R is the radius of the spherical cap (see Fig. 1). L and R are related by eqn (3). For a given set of values for κ, κ_G and A, the energy is a function of r with the free parameter γ. Fig. 7 shows the plot of the energy *versus* r for pored membranes with budding (black curve) and flat (blue curve) pores. The shape of a vesicle with flat pores is approximated as a spherical cap.[47] Fig. 7 shows that for a specified value for the line tension the pore vanishes in both cases in the ground state. We notice that a budding pore has a meta-stable state at about $r = 0.43$. However, this meta-stable state may be hard to see in an experiment, because the depth of the energy barrier ($\sim 0.01\kappa$) is very shallow and the range of values of the line

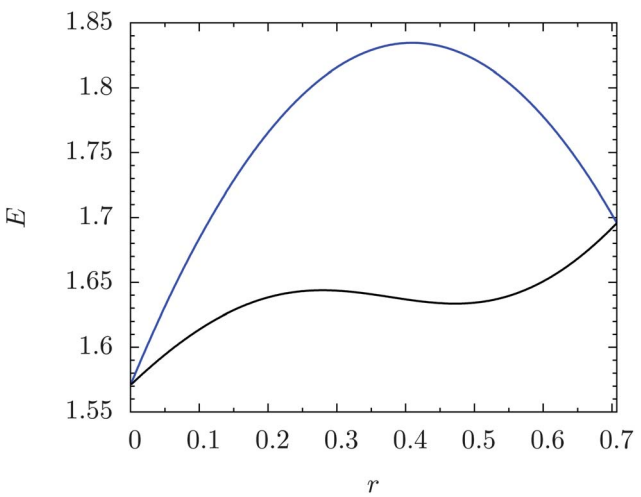

Fig. 7 The plot of energy *versus* the radius of the pore r for membranes with budding (black curve) and flat (blue curve) pores. The two curves coincide at $r = \sqrt{2}/2 \approx 0.7$. It corresponds to a hemisphere beyond which the ansatz shape of a spherical cap plus catenoid does not apply. $\gamma = 0.2049$. $\kappa = 1$, $\kappa_G = 0$, $A = \pi$. The radius of the pore r is measured in the unit of the radius r_0 of the circular disk whose area is fixed in the evolution. The meta-stable pore has $r = 0.43$, so the corresponding radius of the spherical cap is $R = 0.50$, $L = 0.17$, and $\theta = 68$ degrees.

tension where a meta-stable pore exists is very narrow: $0.19 \lesssim r_0\gamma/\kappa \lesssim 0.22$, where r_0 is the radius of the circular disk as defined in the caption of Fig. 7. We perform a series of simulations using Surface Evolver by adding the line energy to the pore. We were not able to observe a stable pore, *i.e.*, the pore either shrinks and closes up (for large values of line tension) or it fully opens and the membrane takes a form of a flat disk (for small line tension). While our numerical results cannot exclude the possibility of the existence of a stable pore within a certain parameter region, they suggest that even if such a region exists, it is very narrow. Therefore, stabilizing agents like talin proteins used in the experiment of ref. 5 are essential for a stable pore on fluid membranes.

3.3. Two-component membrane

So far, we have studied the effects of the mean curvature and the Gaussian curvature terms in the Helfrich free energy on the shape of pored membranes. It is interesting to extend the flattening effect due to the Gaussian curvature to two-component membranes where the components' Gaussian rigidities are different. A pored membrane may be regarded as a limiting case of a two-component membrane, where one phase has vanishing bending and Gaussian rigidities. The effect of the inhomogeneity of the Gaussian rigidity in multicomponent membranes has been extensively discussed.[23,31,37,41,42] Monte Carlo simulations show that a difference in the Gaussian rigidity of a two-component membrane can develop and stabilize multi-domain morphologies.[23,41,42] An explicit analytical expression for the shapes of axisymmetric closed membranes with multiple domains was derived in ref. 37. However, the influence of the inhomogeneity of the Gaussian curvature on the local shape near the phase boundary was not explicitly discussed. In this subsection, we study how the same Gaussian-curvature effect that leads to the flattening near a pore can result in the onset of budding in a multicomponent membrane, if the Gaussian rigidities of the components are different. For simplicity, consider a two-component spherical membrane with Gaussian rigidities $\kappa_G^{(1)}$ and $\kappa_G^{(2)}$ for domain 1 and domain 2 of the sphere, respectively (see Fig. 8). Suppose $\Delta\kappa_G = \kappa_G^{(2)} - \kappa_G^{(1)} > 0$ without loss of generality. The integral of the Gaussian curvature over the whole surface is $\kappa_G^{(1)}\int_1 K_G dA + \kappa_G^{(2)}\int_2 K_G dA = 2\pi(\kappa_G^{(1)} + \kappa_G^{(2)}) - \Delta\kappa_G\oint_2 k_g dl = 2\pi(\kappa_G^{(1)} + \kappa_G^{(2)}) + \Delta\kappa_G\oint_1 k_g dl$, where the subscript numbers in the line integrals represent the boundary of the respective domains. The second and third expressions indicate that the geodesic curvature on the boundary of domain 2 (with larger Gaussian rigidity) prefers to increase and that on the boundary of domain 1 (with smaller Gaussian rigidity) prefers to decrease for lowering the Helfrich free energy. The effect is similar to imposing a "torque" rotating outward the original shape near the boundary loop (the dashed lines in Fig. 8).

In order to confirm the proposed budding scenario, we performed a series of simulated annealing Monte Carlo simulations for a triangulated two-component membrane. Components were assigned to the vertices of the discrete mesh and liquid character of the membrane is ensured by using a dynamical triangulation; *i.e.*, we employed a Monte Carlo move in which an edge shared by two triangles was flipped to connect two vertices that were previously not connected.[8,43] The discrete version of the mean curvature term in the Helfrich free energy was calculated following a prescription introduced by Gompper and Kroll,[44] while the Gaussian curvature term was treated according to Meyer *et al.*[45] For a membrane with about 2×10^3 vertices typically 10^5 Monte Carlo sweeps with a linear cooling protocol were sufficient to obtain low energy structures, with a sweep defined as an attempted move of each vertex followed by an attempted flip of each edge.

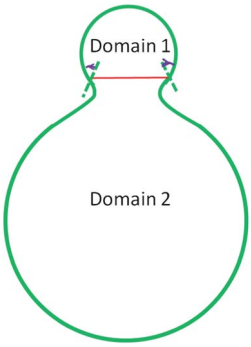

Fig. 8 The schematic plot of budding on a two-component membrane. The red line represents the boundary of the two domains. $|\kappa_G^1| > |\kappa_G^2|$.

The result is shown in Fig. 9. In the simulation, $\kappa = 2$, $\kappa_G^{(2)} = -0.5$ and $\kappa_G^{(1)}/\kappa_G^{(2)}$ increases from unity to 6. The deviation from a spherical shape is characterized by the asphericity $\frac{\langle(\Delta R)^2\rangle}{\langle R\rangle^2} = \frac{1}{N}\sum_{i=1}^{N}\frac{(R_i - \langle R\rangle)^2}{\langle R\rangle^2}$, where R_i is the radial distance of vertex i and $\langle R\rangle = \frac{1}{N}\sum_{i=1}^{N} R_i$ is the mean radius.[46] With the increasing inhomogeneity in the Gaussian rigidity, the "torque" imposed on the phase boundary becomes stronger and budding of the smaller component becomes more obvious as shown in Fig. 9. This budding mechanism arising from an inhomogeneity in the Gaussian rigidity is distinct from the usual mechanism due to line tension. It sheds light on understanding shapes of

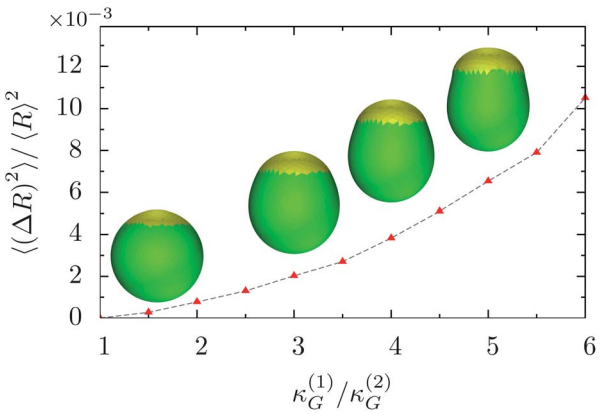

Fig. 9 The plot of the asphericity of a two-component membrane *vs.* the ratio of the two Gaussian rigidities in the two-component membrane with 15% of the purple (domain 1) component. Budding becomes more obvious with the increase of the inhomogeneity of the membrane in Gaussian rigidity.

multicomponent membranes and provides a novel method to control the shape of membranes.

4. Conclusions

Our study of shapes of pored membranes of fixed area and pore size within the framework of the Helfrich theory shows that the presence of pores can be an important ingredient for generating various shapes of membranes. Several structures brought by pores have been disclosed, including the budding pores purely due to the mean curvature term and the flattening effect due to the Gaussian curvature term. The latter effect may be used to fabricate pore-controlled buckled membranes. Furthermore, we have proposed a method to extract the value of the Gaussian rigidity of a membrane simply from its shape. This scheme may be generalized to systems where the elastic moduli are difficult to measure, like in living materials. In addition, by relaxing the constraint of a fixed pore size and adding the line tension, we briefly discuss the stability of a pore and find that a budding pore may be meta-stable with a very shallow energy barrier within a narrow range of line tension values. Finally, we extend the flattening effect due to the Gaussian curvature as found in studying pored membranes to two-component membranes. Theoretical analysis shows that sufficiently high contrast between the components' Gaussian rigidities can lead to budding of a two-component membrane, which is substantiated by MC simulations.

Acknowledgements

Numerical simulations were in part performed using the Northwestern University High Performance Computing Cluster Quest. ZY, MO and CT thank the financial support of the Air Force Office of Scientific Research (AFOSR) under Award No. FA9550-10-1-0167. RS and MO thank the financial support of the US Department of Energy Award DEFG02-08ER46539.

References

1 B. Alberts, A. Johnson, J. Lewis, M. Raff, K. Roberts, P. Walter, D. Bray and J. D. Watson, *Molecular Biology of the Cell*, Garland Science, New York, 5th edn, 2007.
2 R. Lipowsky and E. Sackmann, *Structure and Dynamics of Membranes*, Elsevier, 1995.
3 D. L. Nelson and M. M. Cox, *Lehninger Principles of Biochemistry*, W. H. Freeman, New York, 4th ed., 2005.
4 D. Lingwood and K. Simons, *Science*, 2009, **327**, 46.
5 A. Saitoh, K. Takiguchi, Y. Tanaka and H. Hotani, *Proc. Natl. Acad. Sci. U. S. A.*, 1998, **95**, 1026.
6 B. Fourcade, M. Mutz and D. Bensimon, *Phys. Rev. Lett.*, 1992, **68**, 2551.
7 X. Michalet and D. Bensimon, *Phys. Rev. Lett.*, 1994, **72**, 168.
8 D. R. Nelson, T. Piran and S. Weinberg, *Statistical Mechanics of Membranes and Surfaces*, World Scientific, Singapore, 2nd edn, 2004.
9 Z. C. Ou-Yang and W. Helfrich, *Phys. Rev. A*, 1989, **39**, 5280.
10 R. Lipowsky, *Nature*, 1991, **349**, 475.
11 W. Helfrich, *Zeitschrift Für Naturforschung C-A Journal of Biosciences*, 1973, **28**, 693–703.
12 Z. C. Ou-Yang, J. X. Liu and Y. Z. Xie, *Geometric Methods in the Elastic Theory of Membranes in Liquid Crystal Phases*, World Scientific Publishing Company, 1999.
13 S. A. Safran, *Statistical Thermodynamics of Surfaces, Interfaces, and Membranes*, Westview Press, Colorado, 2003.
14 H. J. Deuling and W. Helfrich, *Biophys. J.*, 1976, **16**(8), 861.
15 W. Helfrich, *Z. Naturforsch., A: Phys. Sci.*, 1978, **33**, 305.
16 R. J. C. Gilbert, *Cell. Mol. Life Sci.*, 2002, **59**, 832.
17 F. Bonardi, E. Halza, M. Walko, F. Du Plessis, N. Nouwen, B. L. Feringa and A. J. M. Driessen, *Proc. Natl. Acad. Sci. U. S. A.*, 2011, **108**, 7775.
18 F. Nomura, M. Nagata, T. Inaba, H. Hiramatsu, H. Hotani and K. Takiguchi, *Proc. Natl. Acad. Sci. U. S. A.*, 2001, **98**, 2340.
19 M. Dubois, B. Deme, T. Gulik-Krzywicki, J. C. Dedieu, C. Vautrin, S. Desert, E. Perez and T. Zemb, *Nature*, 2001, **411**, 672–675.
20 M. Hu, J. J. Briguglio and M. Deserno, *Biophys. J.*, 2012, **102**, 1403.
21 K. Brakke, *Exp. Math.*, 1992, **1**, 141–165.
22 K. Brakke, http://www.susqu.edu/brakke/evolver/evolver.html.
23 J. Hu, T. Weikl and R. Lipowsky, *Soft Matter*, 2011, **7**, 6092.
24 M. F. Demers, R. Sknepnek and M. Olvera de la Cruz, *Phys. Rev. E: Stat., Nonlinear, Soft Matter Phys.*, 2012, **86**, 021504.
25 G. Vernizzi, R. Sknepnek and M. Olvera de la Cruz, *Proc. Natl. Acad. Sci. U. S. A.*, 2011, **108**, 4292–4296.
26 R. Sknepnek, G. Vernizzi and M. Olvera de la Cruz, *Soft Matter*, 2012, **8**, 636.
27 R. Sknepnek and M. Olvera de la Cruz, *Phys. Rev. E: Stat., Nonlinear, Soft Matter Phys.*, 2012, **85**, 050501(R).
28 R. Lipwsky, *Biophys. J.*, 1993, **64**, 1133.
29 T. Kohyama, D. M. Kroll and G. Gompper, *Phys. Rev. E: Stat., Nonlinear, Soft Matter Phys.*, 2003, **68**, 061905.
30 P. Méléard, J. Faucon, M. Mitov and P. Bothorel, *Europhys. Lett.*, 1992, **19**, 267.
31 T. Baumgart, S. Das, W. W. Webb and J. T. Jenkins, *Biophys. J.*, 2005, **89**, 1067.
32 D. J. Struik, *Lectures on Classical Differential Geometry*, Dover Publications, 2nd edn, 1988.
33 J. C. C. Nitsche, *Lectures on Minimal Surfaces*, Cambridge University Press, 1989.
34 P. A. Kralchevsky and K. Nagayama, *Particles at Fluid Interfaces and Membranes*, Elsevier, 2001.
35 R. Templer, B. Khoo and J. Seddon, *Langmuir*, 1998, **14**, 7427–7434.
36 T. Umeda, Y. Suezaki, K. Takiguchi and H. Hotani, *Phys. Rev. E: Stat., Nonlinear, Soft Matter Phys.*, 2005, **71**, 011913.
37 T. Idema and C. Storm, *Eur. Phys. J. E: Soft Matter Biol. Phys.*, 2011, **34**, 1–10.
38 S. Semrau, T. Idema, L. Holtzer, T. Schmidt and C. Storm, *Phys. Rev. Lett.*, 2006, **100**, 088101.
39 Y. C. Fung, *Biomechanics: Mechanical Properties of Living Tissues*, Springer, 2nd edn, 1993.
40 A. J. Crosby and J. J. McManus, *Phys. Today*, 2011, **64**, 62.
41 J. Allain, C. Storm, A. Roux, M. Amar and J. Joanny, *Phys. Rev. Lett.*, 2004, **93**, 158104.
42 F. Jülicher and R. Lipowsky, *Phys. Rev. Lett.*, 1993, **70**, 2964–2967.
43 V. A. Kazakov, I. Kostov and A. Migdal, *Phys. Lett. B*, 1985, **157**, 295–300.
44 G. Gompper and D. Kroll, *J. Phys. I*, 1996, **6**, 1305–1320.
45 M. Meyer, M. Desbrun, P. Schröder and A. H. Barr, *Visualization and Mathematics*, 2002, **3**, 34–57.
46 J. Lidmar, L. Mirny and D. R. Nelson, *Phys. Rev. E: Stat., Nonlinear, Soft Matter Phys.*, 2003, **68**, 051910.
47 W. Helfrich, *Phys. Lett. A*, 1974, **50**, 115–116.